Characterization of $Si/Si_{1-x}Ge_x/Si$ quantum wells by space-charge spectroscopy

K. Schmalz
Institute of Semiconductor Physics, PF 409, W.-Korsing-Strasse 2, D-15204 Frankfurt (Oder), Germany

I. N. Yassievich
A. F. Ioffe Physico-Technical Institute, Polytechnicheskaya 26, St. Petersburg 194021, Russia

H. Rücker
Institute of Semiconductor Physics, PF 409, W.-Korsing-Strasse 2, D-15204 Frankfurt (Oder), Germany

H. G. Grimmeiss
University of Lund, Department of Solid State Physics, P.O. Box 118, S-22100 Lund, Sweden

H. Frankenfeld, W. Mehr, H. J. Osten, P. Schley, and H. P. Zeindl
Institute of Semiconductor Physics, PF 409, W.-Korsing-Strasse 2, D-15204 Frankfurt (Oder), Germany
(Received 30 November 1993; revised manuscript received 13 July 1994)

Results are presented concerning the electrical characterization of p-$Si/Si_{1-x}Ge_x/Si$ quantum well (QW) structures by admittance spectroscopy, capacitance measurements, and deep-level transient spectroscopy (DLTS). The capture and emission processes of holes in QW structures are theoretically analyzed for equilibrium and nonequilibrium conditions taking into account external electric fields as well as local electric fields induced by confined charge carriers. The temperature dependence of potential barriers at the QW and of the Fermi level determines the activation energy E_a of the conductance across the QW. Admittance spectroscopy data of QW's with $x=0.25$ and thicknesses in the range from 1 to 5 nm are in fair agreement with the proposed theoretical model. Hole emission from the QW region was studied by DLTS investigations on n^+p mesa diodes for QW's with $x=0.17$.

I. INTRODUCTION

The band offset of semiconductor quantum well (QW) structures is often determined by means of different optical and electrical methods.[1] Due to the fact that these methods do not allow us to measure the band offset directly, the different techniques and, in particular, the analysis of the data obtained have to be evaluated very carefully.

Junction space-charge techniques (JSCT), such as capacitance-voltage investigations (CV), admittance spectroscopy, and deep-level transient spectroscopy (DLTS), are relatively simple techniques regarding the experimental facilities and the analysis of data. Hence, semiconductor quantum well structures as part of a depletion region of a diode should be easily investigated by different space-charge techniques. The CV-method reveals the profile of carrier concentrations within the space-charge region of a pn or Schottky diode. Admittance spectroscopy[2] and DLTS (Ref. 2) are in this context similar dynamic techniques for the investigation of carrier capture and emission in quantum wells (QW). The admittance spectroscopy measures the charge-carrier transport over the QW, and DLTS monitors the carrier emission from the QW.

Using simple thermionic emission theory[3] for describing carrier transport across potential barriers, it is readily shown that the thermally activated current is limited in both cases by a potential barrier closely related to the band offset ΔE. Several DLTS investigations[2,4–7] and admittance spectroscopy measurements[2,8] have been published for semiconductor heterostructures to obtain information on ΔE.

In the case of admittance spectroscopy, the QW should be situated in the neutral region of the semiconductor diode, whereas for DLTS measurements the QW should be located in the space-charge region of the diode at least during the carrier emission process. A drawback of DLTS investigations is the strong influence of the electric field in the space-charge region on the carrier emission,[2] since the potential barrier at the QW is considerably decreased due to high electric fields. Furthermore, the internal electric field induced by confined charge carriers has to be considered in the case of capture processes and the induced potential barriers must be taken into account in the analysis of carrier transport across the QW. Previous publications[2,4,7] have not considered the pecularities of carrier capture and emission in QW's which are related to quantum effects.

Deep-level transient spectroscopy investigations of the band offset of QW structures in $A_{III}B_V$ semiconductors[4,7,9] give rather contradictory results. Using these DLTS results only it is not possible to conclude whether direct carrier emission from the QW or emissions from defect levels in the QW were observed. A better interpretation is possible, if DLTS, CV, and admittance spectroscopy measurements were performed on similar device structures or, as in,[5] if CV measurements are used to show that carriers are really confined in the QW.

0163-1829/94/50(19)/14287(15)/$06.00

Recently, an increasing technological interest in $Si/Si_{1-x}Ge_x$ heterostructure layers has been observed due to possible applications in silicon based device technology.[10] When studying carrier emission from QW's in $Si/Si_{1-x}Ge_x/Si$ QW structures, it is of interest to note that, in contrast to $A_{III}B_V$-semiconductor heterostructures, only the offset of the valence band is essential, and that the concentration of deep centers in the $Si/Si_{1-x}Ge_x/Si$ layers should be small. Admittance spectroscopy measurements of the valence-band offset ΔE_V have previously been performed on p-type $Si/Si_{1-x}Ge_x/Si$ QW structures for Ge concentrations up to 30 at. %,[8] but the analysis was performed without taking into account the potential barrier induced by confined carriers. Recently, DLTS investigations on structures with $x=0.3$ have shown a rather broadband in the DLTS spectrum at lower temperatures, which was assumed to be due to direct hole emission from the QW.[6]

The aim of this paper is to present a detailed theoretical and experimental study of carrier capture and emission processes in p-type $Si/Si_{1-x}Ge_x/Si$ QW structures. The experimental study combined CV, admittance, and DLTS measurements of similar structures in order to obtain reliable information on electronic parameters of the QW structures, such as the acceptor concentration, the concentration of confined holes, the activation energy of conductance across the QW, as well as the activation energy of carrier emission from the QW.

The carriers confined by the QW induce local electric field, which change the capture and emission processes considerably. The strength of these fields depends on the QW parameters as well as on the doping concentration and the concentration of confined carriers. A detailed investigation of such effects for p-$Si/Si_{1-x}Ge_x/Si$ structures is presented.

The paper is organized as follows. The theoretical study is presented in Sec. II. Section III describes the experimental procedures and the sample preparation. A discussion of experimental and theoretical results is given in Sec. IV. Finally, the most important conclusions are summarized in Sec. V.

II. THEORETICAL STUDY OF CAPTURE AND EMISSION PROCESSES

The valence- and conduction-band discontinuities in $Si/Si_{1-x}Ge_x/Si$ QW structures are strongly dependent on the alloy composition of the individual layers as well as on the actual strain situation. Strained $Si_{1-x}Ge_x$ QW layers embedded in unstrained Si, which will be studied here, represent deep traps for holes whereas the confinement of electrons is less important. The variation of the band offset with respect to the actual strain situation and the Ge content x in the QW can be estimated from the deformation-potential theory combined with a virtual-crystal approximation for the alloy layers (see Appendix A). Figure 1 shows the position of the highest valence bands and lowest conduction bands of strained $Si_{1-x}Ge_x$ layers, pseudomorphically grown on Si substrates, relative to the Si band edges. We have adopted here the results of *ab initio* calculations from Van de Walle and Martin[20] for the deformation potentials and for the valence-band offset of the strained Ge matched to a Si(001) substrate.

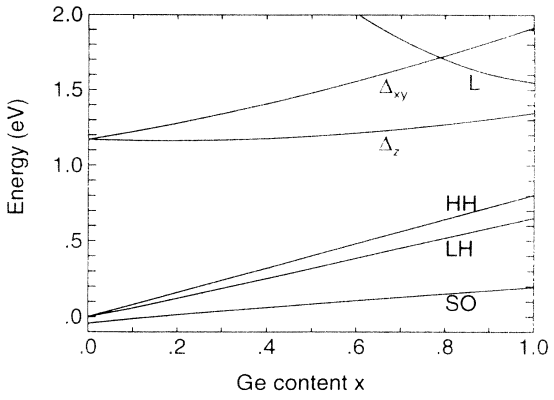

FIG. 1. Band edges of a strained $Si_{1-x}Ge_x$ layer matched to a Si(001) substrate versus x. Heavy holes (HH), light holes (LH), and holes slit off by spin-orbit coupling (SO) as well as the L valley and the inequivalent Δ valleys are plotted relative to the Si valence-band edge.

To obtain the valence-band offset from the experimental results of space-charge spectroscopy measurements,[2] it is necessary to examine capture and emission processes of holes in the QW for equilibrium and nonequilibrium conditions carefully and to take into account external electric fields as well as local electric fields induced by confined holes. The understanding of these processes is important for device applications as well.

A. The flat band case

From the classical point of view, a quantum well in a sample structure used here presents a giant trap for holes. The density of the emission current is given by

$$j_e = e_T n_w \ , \tag{1}$$

where e_T is the thermal emission rate and n_w is the two-dimensional hole concentration in the QW.

In thermionic theory it is assumed that all carriers in the well with energies larger than ΔE_v can leave the well without any obstacles. In this way, all free carriers arriving at the boundary of the well are captured by the well, which means that the density of the capture flux is given by

$$j_c = 2 n_b \langle v \rangle \ , \tag{2}$$

where n_b is the free-carrier concentration in the barrier layer close to the well and $\langle v \rangle = (8 k_B T/\pi m)^{1/2}$ is the average thermal velocity of carriers with mass m at temperature T. The factor 2 in Eq. (2) accounts for the capture from both sides of the well. In thermal equilibrium, when the same Fermi level determines the occupation of states in the barrier layers and in the well, we have $j_c = j_e$.

The equilibrium concentrations of holes in a QW with confinement energies E_n is given by

$$n_w=\frac{mk_BT}{\pi\hbar^2}\sum_n \ln\left[1+\exp\left[\frac{E_F-E_{vw}-E_n}{k_BT}\right]\right], \quad (3)$$

where E_F is the Fermi level for holes and E_{vw} and E_{vb} are the valence-band edges of the well and the barrier, respectively. The valence-band offset is defined as $\Delta E_v=E_{vb}-E_{vw}$. In the case of Boltzmann statistics, the carrier density in the well is

$$n_w=\frac{mk_BT}{\pi\hbar^2}\exp\left[\frac{E_F-E_{vw}}{k_BT}\right]\sum_n \exp\left[\frac{-E_n}{k_BT}\right]. \quad (4)$$

From the thermal equilibrium condition for the capture and emission fluxes, the emission rate is obtained as

$$e_T=\frac{2\langle v\rangle}{f\lambda_T}\exp\left[-\frac{\Delta E_v-E_1}{k_BT}\right], \quad (5)$$

where λ_T is the thermal length $\lambda_T=(2\pi\hbar^2/mk_BT)^{1/2}$, and the occupation factor f given by

$$f=\sum_n \ln\left[1+\exp\left[\frac{E_F-E_{vw}-E_n}{k_BT}\right]\right]\exp\left[\frac{E_1}{k_BT}\right] \quad (6)$$

accounts for the degeneration in the QW. Boltzmann statistics then gives

$$f=\sum_n \exp\left[\frac{E_1-E_n}{k_BT}\right]. \quad (7)$$

Here, E_1 is the confinement energy of the first level in the well. In the limit of small wells ($E_1 \gg k_BT$), Eq. (7) reduces to $f=1$ and in the opposite limit of wide wells ($E_1 \ll k_BT$), we have $f=a/\lambda_T$ with a being the width of the well.

When captured in the well, an arriving carrier loses energy. The most effective process of energy dissipation is the emission of optical phonons. If the well width a is less than the mean free path l limited by optical-phonon emission, only a part of the arriving carriers is captured, and the density of capture flux is

$$j_c=2n_b\langle v\rangle a/l. \quad (8)$$

Obviously, the emission rate should involve the same factor a/l.

The main difference of a quantum well compared to the classical well consists in the existence of bound states in the QW and quasistationary levels in the continuum spectrum induced by the reflection of carriers at the QW boundaries. The existence of quasistationary states produces "windows of transparency" for incoming electrons. This fact together with the existence of discrete bound states in the QW leads to an oscillating dependence of emission and capture rates on the well width a (see Ref. 2 and references therein). The basic result is to replace the thermal average velocity $\langle v\rangle$ in Eqs. (2) and (5) by an effective capture velocity v_c, which accounts for optical-phonon emission and is calculated in the framework of quantum theory.[11–13] In the nonpolar $Si/Si_{1-x}Ge_x/Si$ QW structures, where the deformation potentials control the interaction of carriers with optical phonons, the capture velocity for a well with $\Delta E_v=140$ meV and a width of about 30 nm changes between 0.5×10^6 cm/s (minimum at $a\approx29$ nm) and 4×10^6 cm/s (maximum at $a\approx31$ nm) and is practically temperature independent in the region from 100 to 200 K.[11,12]

B. The effect of band bending on capture and emission

For p-type $Si/Si_{1-x}Ge_x/Si$ QW structures with large barrier layers which determine the position of the Fermi level, the confined holes in the QW produce a depletion region in the vicinity of the QW due to the charge neutrality condition. As a result, the bottom of the QW is down shifted, and an electric potential barrier eU_0 appears. The spacial variation of the valence-band edge of a $Si/Si_{0.83}Ge_{0.17}/Si$ QW with $\Delta E_v=140$ meV is shown in Fig. 2 for an acceptor concentration $N_A=10^{17}$ cm^{-3} and $T=100$ K. The bound states as well as the quasibound states in the QW (below the barrier) are indicated for heavy (solid lines) and light (dashed lines) holes, respectively.

The energy levels and the charge density were calculated solving the Schrödinger's and Poisson's equations self-consistently (see Appendix A).

The hole density n_w in a QW surrounded by p-doped barrier layers determines an electric field

$$F_0=\frac{en_w}{2\varepsilon_r\varepsilon_0} \quad (9)$$

at the boundaries of the QW, where $\varepsilon_r\varepsilon_0$ is the dielectric constant and e is the unit charge. The potential barrier U_0 for a given acceptor concentration N_A can be expressed by the hole density n_w as

$$U_0=\frac{en_w^2}{8\varepsilon_r\varepsilon_0N_A}. \quad (10)$$

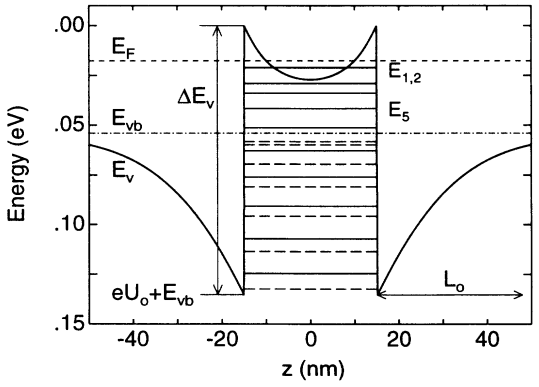

FIG. 2. Valence-band profile in a 30-nm $Si/Si_{0.83}Ge_{0.17}/Si$ QW with an acceptor concentration $N_A=10^{17}$ cm^{-3} and $T=100$ K. Bound states and quasibound states in the QW are shown for heavy (full lines) and light holes (dashed lines). The Fermi energy E_F (dashed) and the valence-band edge E_{vb} in the bulk region (dot dash) are shown. The indicated barrier width L_0 corresponds to the depletion approximation.

Equations (9) and (10) were derived under the assumption of a space-charge depletion layer. It should be noted that the levels of the confined carriers are considerably shifted by the electrostatic potential of the confined charge. The energy levels of confined heavy holes in a $Si/Si_{0.83}Ge_{0.17}$ QW are shown in Fig. 3 as a function of the acceptor concentration N_A in the Si barriers. The limiting energy for bound hole states in the well is given by the valence-band edge E_{vb} in the barrier outside the space-charge region. The most important effect of the electrostatic potential is a shift of all confined levels due to the spacial variation of valence-band edge at the well. With increasing band bending, corresponding to higher doping concentrations, the first and second subbands representing symmetric and antisymmetric combinations of states localized at the boundaries of the well become degenerate. Light-hole levels have not been plotted since in the structure considered, light holes do not contribute to the charge accumulation in the well. Due to the strain imposed by the pseudomorphic growth on Si substrates they are shifted by about 100 meV and, hence, there are no bound light-hole states within the QW. However, it should be noted, that the parallel transport of heavy holes is controlled by the effective mass of light holes (see Appendix A). In the two-dimensional hole density we have therefore used $m=m_l$, where m_l is the effective mass of light holes.

The temperature dependence of the potential barrier eU_0 relative to the Fermi level E_F in the barrier layers is exhibited in Fig. 4 for different acceptor concentrations in the barrier layers. The decreasing potential difference $(eU_0+E_{vb}-E_F)$ with decreasing temperature is mainly caused by a shift of the Fermi level in the barrier layer. The charge transfer between the well and barrier layers aligns the Fermi level of the barriers close to the energy of the first heavy-hole level in the well where the density of states is high.

The local electric field of the order of $10^4,\ldots,10^5$ V/cm induced by the confined charge, and the corresponding approximately parabolic barrier which has a value of about $eU_0=100$ meV, change dramatically the rate of carrier emission and capture processes. If tunneling of holes across the barriers is not considered, an activation law for the thermal emission rate is obtained similar to the flat band case Eq. (5), where the shift of the confined hole levels has to be taken into account. For capture processes an effective velocity v_c^{eff} can be introduced by the relation

$$j_c=v_c^{\text{eff}}n_b\ , \tag{11}$$

where $n_b=N_v\exp[(E_F-E_{vb})/k_BT]$ is the hole concentration in the neutral region of the barrier layer and

$$v_c^{\text{eff}}=v_c\exp\left[-\frac{eU_0}{k_BT}\right]\ . \tag{12}$$

N_v is the effective density of states of the valence band and v_c is the QW capture velocity in the QW obtained under flat band condition (see Chap. 2.1.).

For samples with high doping concentrations and, consequently, narrow barrier regions the tunneling across the barriers can no longer be neglected. For the considered case of $\Delta E_v=0.14$ eV, $a=30$ nm, and $N_A=10^{17}$ cm^{-3} we have a barrier of $eU_0=0.081$ eV (see Fig. 2), and obtain therefore for the depletion width of the barrier $L_0=(2\varepsilon_0\varepsilon_r U_0/eN_A)^{1/2}$ a value of $L_0=33$ nm. This width is somewhat smaller than the depletion width obtained by solving Poisson's equation exactly (see Fig. 2). The probability of tunneling from the quasistationary level E_m depends on the energy distance between E_m and the top of the barrier, i.e., ΔE_v-E_m, and increases for larger E_m. On the other hand, the population of the level decreases for larger value of E_m. There is therefore an optimal energy for tunneling, E^{opt}, which depends on the temperature, and determines the value of the thermally activated tunneling emission rate e_{tu}. In Appendix B, the following relation for e_{tu} is obtained:

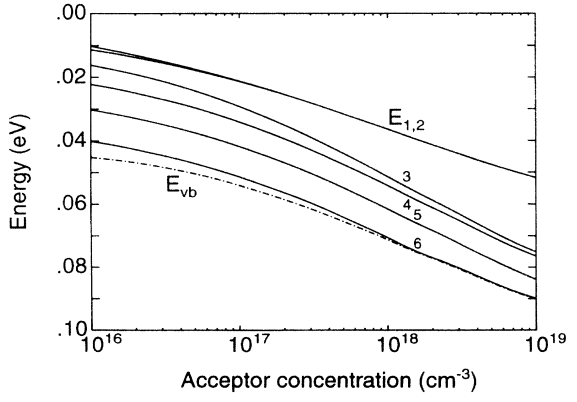

FIG. 3. Energy levels of confined heavy holes in a 30-nm $Si/Si_{0.83}Ge_{0.17}/Si$ QW versus the doping concentration N_A for $T=100$ K. The dot-dash line gives the limiting energy E_{vb} for bound hole states. Energies are measured relative to the bottom of the well.

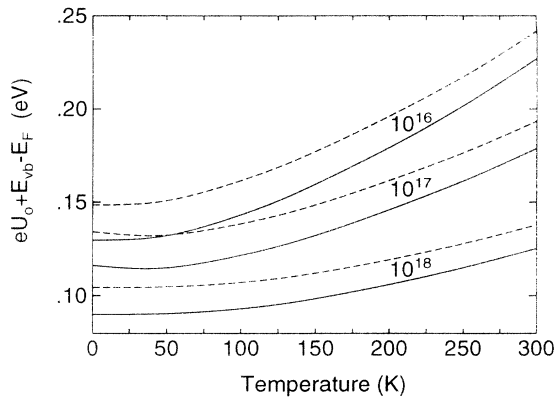

FIG. 4. Potential difference $eU_0+E_{vb}-E_F$ of a 30-nm $Si/Si_{0.83}Ge_{0.17}/Si$ QW versus temperature for different acceptor concentrations $N_A=10^{16}$ cm^{-3}, 10^{17} cm^{-3}, and 10^{18} cm^{-3}, respectively. Valence-band offsets of $\Delta E_V=0.14$ eV (solid lines) and $\Delta E_V=0.16$ eV (dashed lines) were assumed.

$$e_{tu}=\frac{\tilde{\nu}}{T(E^{opt})}\exp\left[\frac{-eU_0}{E_t}th\left[\frac{E_t}{k_BT}\right]\right]\times\exp\left[\frac{-\Delta E_v-E_1}{k_BT}\right]f^{-1}, \quad (13)$$

where $E_t=(e^2N_A\hbar^2/4\varepsilon_r\varepsilon_0 m)^{1/2}$.

$T(E^{opt})$ is the classical period of movement in the quasistationary state at the optimal tunneling energy E^{opt} and ν is the number of quasistationary states contributing to the thermally activated tunneling. Neglecting, in a first approximation, the bending of the QW bottom one obtains

$$T(E^{opt})=a\left[\frac{2m}{E^{opt}}\right]^{1/2}. \quad (14)$$

The importance of tunneling processes is determined by the characteristic energy E_t depending only on the acceptor concentration. For $E_t \ll k_BT$ Eq. (13) transforms into the activation law (5). On the other hand, for $E_t \gg k_BT$ the emission process is controlled by tunneling from the quasistationary levels near the valence band edge in the neutral region.

According to the definition of the energy E_t a value of $E_t \approx 3$ meV is obtained for $N_A=10^{17}$ cm^{-3}, and $E_t \approx 9$ meV for $N_A=10^{18}$ cm^{-3}. Hence, for QW structures with a dopant concentration N_A less than 10^{17} cm^{-3} Eq. (5) can be used for describing the emission process. However, for $N_A \geq 10^{18}$ cm^{-3} tunneling processes become important at temperatures smaller than 100 K. When tunneling is important the effective capture velocity [see Eq. (12)] is given by

$$v_c^{eff}=\frac{\tilde{\nu}\lambda_T}{T(E^{opt})}\exp\left[\frac{-eU_0}{E_t}th\left[\frac{E_t}{k_BT}\right]\right]. \quad (15)$$

It the case of QW's with barriers it has been assumed that the tunneling transparency of the barrier is small, and that all carriers arriving at the QW have enough time to lose their energy which implies that the emission and capture rates are independent of the rate of energy relaxation.

C. Emission and capture processes in external electric fields

So far we have discussed equilibrium conditions where capture and emission fluxes cancel each other. By realizing nonequilibrium conditions, for instance, by applying an external electric field, it is possible to investigate the fluxes individually. Changing the applied external electric field from $F=0$ to $F>F_0$, where F_0 is the local electric field induced by the confined holes, a high hole concentration n_w exists in the QW in the presence of an electric field of the order of 10^5 V/cm. In this case, two aspects must be considered: (i) the shift of the energy of the lowest bound states as a function of F, and (ii) the possibility of thermally activated tunneling through the triangular barrier.

The position of the ground state E_1 in the QW in the presence of a high electric field can be approximated by the confinement energy in a triangular well:[14]

$$E_1 \approx \left[\frac{\hbar^2}{2m}\right]^{1/3}\left[\frac{9\pi}{8}eF\right]^{1/2}. \quad (16)$$

The emission rate controlled by thermally activated tunneling is then given for $F>F_0$ by

$$e_T(F)=\frac{\tilde{\nu}}{T(E^{opt})}\exp\left[-\frac{\Delta E_v-E_1}{k_BT}\right]\exp\left[\frac{\hbar^2e^2F^2}{24m(k_BT)^3}\right], \quad (17)$$

where the preexponential factor $\tilde{\nu}/T(E^{opt})$ is defined as in Eq. (13). Equation (17) can be verified in the same way as demonstrated in Appendix B for parabolic barriers (see also Ref. 15).

D. Kinetics of carrier capture

Here we consider the time dependence of the density of capture flux in QW's for p-doped structures. The initial condition corresponds to the absence of carriers in the QW, i.e., $n_w=0$. The change of the carrier concentration in the well is given by

$$dn_w=[j_c(t)-j_e(t)]dt. \quad (18)$$

The capture flux density j_c of thermally activated processes is given by Eqs. (11) and (12), where U_0 should be replaced by $U_0=U_0(t)$, the potential barrier induced by the confined carriers at time t. The emission current density j_e is given by Eq. (5). Taking into account the dependence of the barrier U_0 on the hole density as given by Eq. (10) one obtains

$$n_w(t)=2v_c\int_0^t dt'\left[n_b\exp\left[\frac{-n_w^2(t')e^2}{8\varepsilon_r\varepsilon_0N_Ak_BT}\right]-\frac{n_w(t')}{\lambda_T f}\exp\left[-\frac{\Delta E_v-E_1}{k_BT}\right]\right]. \quad (19)$$

The integral equation (19) determines the time dependence of the hole concentration n_w. The characteristic time for the capture process is

$$\tau_0=\left[\frac{\varepsilon_r\varepsilon_0N_Ak_BT}{2e^2v_c^2n_b^2}\right]^{1/2}.$$

For $t \leq \tau_0$ the population of the QW increases linearly with time. An estimation of the characteristic time for $N_A=10^{17}$ cm^{-3}, $n_b=N_A$, and $T=100$ K gives $\tau_0 \approx 10^{-12}$ s.

Space-charge spectroscopy measurements generally use frequencies in the range from kHz to MHz. Hence, the initial linear time-dependent filling of the well is not observed but it is possible to study the slow increase of the hole concentration in the vicinity of the equilibrium occupation

$$n_w(t)=\bar{n}_w\left[1-\tfrac{1}{2}\exp(-e_Tt)\right], \quad (20)$$

where $\bar{n}_w$ is the equilibrium hole density and the emission rate e_T is given by Eq. 5. Thus, the time dependence of the hole concentration in the well near equilibrium is determined by the reemission of holes, and, hence, the emission rate can be studied by capture processes.

III. EXPERIMENTAL DETAILS

It should noted that studies as discussed here can only be performed in samples with low leakage current. In order to reduce the leakage current over the *p*-type $Si/Si_{1-x}Ge_x/Si$ QW structures a mesa n^+p-diode geometry was developed such that the QW $Si_{1-x}Ge_x$ layer did not penetrate the mesa, but formed a buried layer. Some of the measurements were performed on WTi-Schottky diodes.

The three-chamber molecular-beam epitaxy (MBE) equipment used for the layer deposition for the n^+p-mesa diodes (labeled as DOT samples) has been described elsewhere.[16] *P*-type Si(100) substrates were prepared by an appropriate *ex situ* and *in situ* cleaning procedure, resulting in atomically clean and (2×1) reconstructed silicon surfaces as verified with reflection high-energy electron diffraction. First, a Si buffer layer was deposited at a growth temperature of 600 °C with an electron-beam evaporator. Elemental boron was evaporated from a high-temperature effusion cell with graphite crucible, whereas Ge and Sb were evaporated from conventional water-cooled pyrolitic boron-nitride Knudsen cells. The SiGe layers were grown at a substrate temperature of 500 °C.

The following layer sequence was deposited: 60-nm n^+-Si layer, Sb doped with about 10^{18} cm^{-3}; 150-nm *p*-Si layer, boron doped with about 10^{17} cm^{-3}; 50-nm Si layer, undoped; 30-nm $Si_{1-x}Ge_x$ layer, undoped; 50-nm Si buffer layer, undoped; *p*-Si substrate, (100)-orientated, B doped with 10^{15} cm^{-3} (see Fig. 5).

The size of the substrate samples was 18×25 mm^2. The undoped layers were of *p* type due to the background boron contamination. The concentration of boron at the interface buffer and substrate was at most a few 10^{17} cm^{-3}. Employing mesa technology we prepared n^+p photodiodes on the MBE samples. The depth of the mesa etching was 80 nm. The area of the n^+ contact was $A = 1.2\times10^{-3}$ cm^2, 4.6×10^{-3} cm^2, and 7.5×10^{-5} cm^2, respectively. The surface of the cap layer was passivated with SiO_2 deposited by chemical-vapor deposition (CVD) and the metallization on the n^+ region was performed by a W/Ti deposition followed by a Al deposition. The three diodes of different sizes were located close to each other in an area of 1×1 mm^2 in each case. 1-MHz CV measurements showed that for the same reverse bias U_R the capacitance values of the diodes were proportional to the respective area, indicating that no inversion layers were formed around the n^+ contact. From the current-voltage characteristics, an ideality factor of 1.4–2.0 was observed for the diodes. The serial resistance of the large diodes was about 400 Ω and the experimental investigations described below were therefore performed on the large diodes. The reverse current I_R at $U_R = 2$ V was about 10^{-6} A. For each diode, the Ge concentration of the $Si_{1-x}Ge_x$ layer was controlled by measuring the shift of the Raman peak position of the Si-Si phonon mode and assuming a pseudomorphic growth.[17] The values obtained for the investigated diodes DOT25 and DOT26 are $x = 0.17$ and 0.25, respectively. The accuracy was ±0.01 in x.

Other samples (labeled as VG samples) (Fig. 6) used in this study were grown pseudomorphically in a commercial 4" solid source MBE system VG 80 S. The deposition chamber was equipped with two electron-beam evaporators for silicon and germanium and a convential effusion cell with a graphite crucible for boron doping. Growth rates for Si and Ge were monitored by Sentiell III sensorheads, whereas the doping flux was controlled

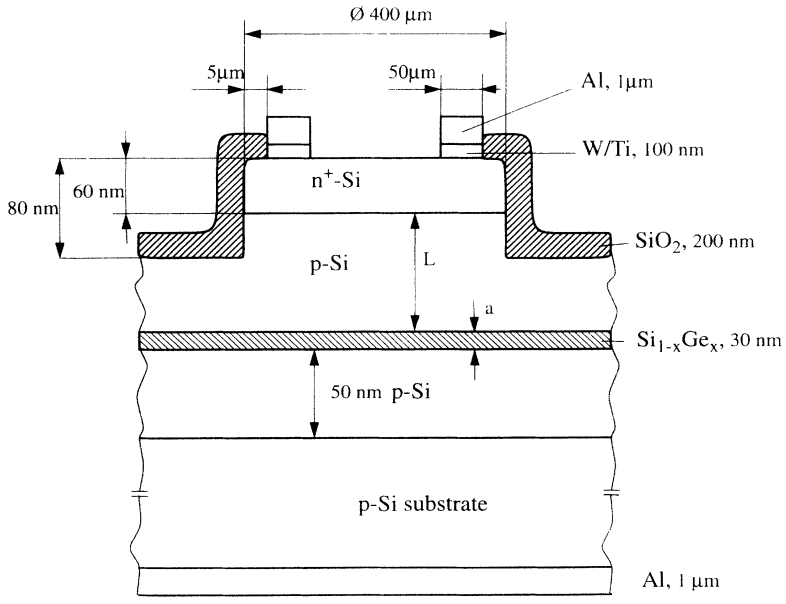

FIG. 5. Schematic picture of the mesa structure used (DOT samples).

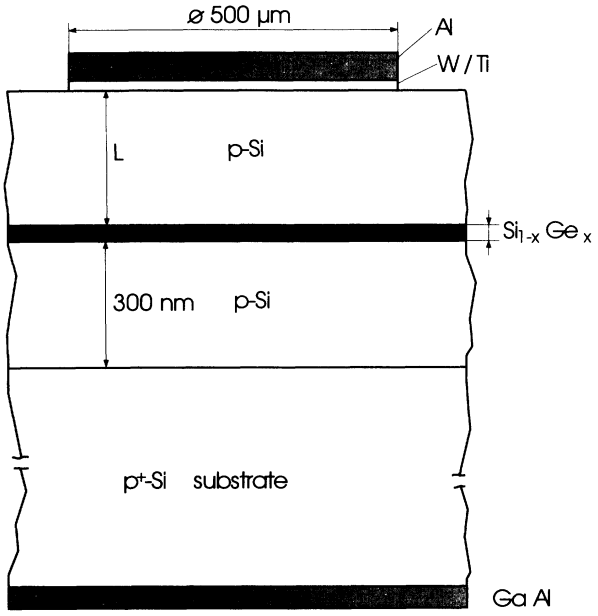

FIG. 6. Schematic picture of the WTi-Schottky diode used (VG samples).

by thermocouples. The epitaxial layers were deposited onto (100) p^+-doped substrates with a resistivity of 0.01–0.02 Ω cm. After desorbing the native oxide *in situ* from the Si substrates by a high-temperature ($T=900$ °C) cleaning step, a 300-nm p-doped (N about 10^{17} cm^{-3}) Si-buffer layer was grown at a substrate temperature of 500 °C. For the individual samples, $Si_{0.75}Ge_{0.25}$ layers with different thicknesses of 1, 2, 3, 5, and 20 nm were sandwiched between 30-nm doped silicon. Finally, a 300-nm-thick p-doped (N about 10^{17} cm^{-3}) Si cap layer was deposited. To control precisely the germanium content as well as the layer thickness of the SiGe layers, thicker samples with the same germanium concentration were investigated by x-ray diffraction methods and the corresponding deposition time for thinner layers was extrapolated. We prepared Schottky diodes on these MBE samples by W/Ti deposition followed by Al deposition. The area of the Schottky contact was $A=1.7\times10^{-3}$ cm^2.

The DLTS measurements were carried out with the commercial DLTS spectrometer DLS-82 of SEMILAB, Hungary and CV and admittance investigations were performed using the low-frequency impedance analyzer HP 4192A.

A. CV measurements

The dependence of the width W of the space-charge layer on the reverse bias U_R was obtained from CV measurements performed at 1 MHz. It was found that for the diodes DOT25 ($x=0.17$) and DOT26 ($x=0.25$) as well as for the Schottky diodes of the VG samples ($x=0.25$) the boron concentration in the Si layer of thickness L above the $Si_{1-x}Ge_x$ layer was large enough to ensure $W(0)<L$ for $U_R=0$ at $T=300$ K (Figs. 5, 6). The profile of the carrier concentration $N=N(W)$ for VG samples obtained from the dependence $C=C(U_R)$ is plotted in Fig. 7. The $N(W)$ profiles for the VG samples gave nearly constant acceptor concentrations N_{A1} and N_{A2} in the B-doped layers above and below the $Si_{1-x}Ge_x$ layer, respectively. $C(U_R)$ measurements were also performed on VG samples, for which surface layers of about 50 and 100 nm were removed by chemically etching to obtain reliable data on N_{A2}. The values of N_{A1} and N_{A2} are given in Table I below. For the DOT samples and all VG samples except the sample with the 1-nm $Si_{1-x}Ge_x$ layer, a concentation peak appears in the $N(W)$ profile in the region of the QW, Fig. 7. The peak corresponding to the region of the $Si_{1-x}Ge_x$ layer seems to be related to hole confinement in the QW,[5] since the CV measurements performed at temperatures from 300 K down to lower temperatures results in profiles expected for an increased apparent hole concentration. The peak shifted to higher depth W at lower temperatures (Fig. 7). It cannot be excluded that the temperature dependent shift of the peak could originate from an RC-time constant effect of the QW.[2] In the temperature and frequency range, where RC-time constant effects are essential, the width W is no longer proportional to the measured inverse capacitance C^{-1} and the determination of the dependence $W=W(U_R)$ is considerably more complicated. Since RC-time constant effects are less important for higher temperatures and lower frequencies, the $W(U_R)$ dependence calculated from CV data at high temperatures was used for the analysis of the DLTS depth profiling discussed below for the DOT25 sample Sec. III C.

In principle, the band offset ΔE_v at the QW layer can be calculated from the profile $N(W)$ measured under conditions not influenced by the RC-time constant effect, if the dopant concentration profile around the QW is known.[18] The concentration n_w of confined holes was obtained from the $C=C(U_R)$ dependence in all those cases where the measurements were not influenced by RC-time constant effects. The dependence $1/C^2$ versus U_R plotted in Fig. 8 for a VG-sample shows a plateau of nearly

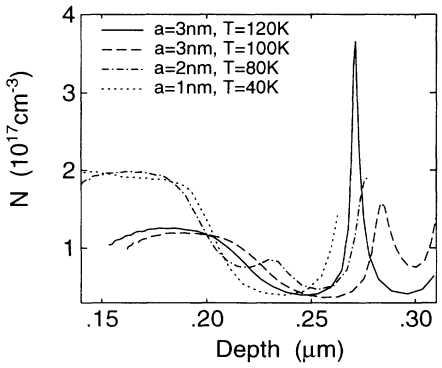

FIG. 7. Apparent carrier concentration profile $N=N(W)$ obtained from 1-MHz CV measurements for different thickness a of the QW at different temperatures [$a=3$ nm, $T=120$ K (solid line); $a=3$ nm, $T=100$ K (dashed line); $a=2$ nm, $T=80$ K (dash-dot line); $a=1$ nm, $T=40$ K (dotted line)].

TABLE I. Experimental results of CV admittance and DLTS measurements.

	Parameters of p-Si/$Si_{1-x}Ge_x$/Si layer			CV results			Admittance results		DLTS
	a (nm)	x	d_{sp} (nm)	N_{A1} (10^{17} cm^{-3})	N_{A2} (10^{17} cm^{-3})	n_w (10^{11} cm^{-2})	L_0 (nm)	E_a (eV)	E_a (eV)
n^+p diodes	30	0.17	50	1	4		55 (130–220 K)	0.14 ±0.01	0.18 ±0.02
	30	0.25	50	0.5	3		47 (117–205 K)	0.15 ±0.01	
WTi-Schottky diodes	1	0.25	30	2.6	3.1		30 (25–31 K)	0.046 ±0.002	
	2	0.25	30	2.0	2.0	0.8±0.5 (110 K)	31 (52–68 K)	0.062 ±0.001	
	3	0.25	30	1.3	2.0	3±0.5 (120 K)	36 (80–105 K)	0.105 ±0.001	
	5	0.25	30	1.4	2.6	3±0.5 (160 K)	39 (111–139 K)	0.143 ±0.007	
	20	0.25	30	3.0	3.0	3±0.5 (190 K)	32 (114–156 K)	0.108 ±0.006	

constant capacitance C^*. The plateau between the first and second critical biases U_{R1} and U_{R2}, respectively, is related to the hole concentration in the QW by $n_w = C^*(U_{R1} - U_{R2})/Ae$,[19] where A is the diode area and e is the elementary charge. The estimated n_w values are presented in Table I.

The CV measurements performed on n^+p diodes allowed only a rough estimate of an acceptor concentration N_A of about 10^{17} cm^{-3} in the vicinity of the quantum well (Table I) and no precise measurement of the confined carrier concentration. A concentration peak of about 3×10^{17} cm^{-3} near the interface between buffer and substrate is related to a boron concentration peak due to a background contamination in the MBE system as observed by secondary-ion-mass spectroscopy measurements.

B. Admittance spectroscopy investigations

The temperature dependence of the diode capacitance $C = C(T)$ is qualitatively different for QW layers located in the neutral region and in the space-charge region of the n^+p or Schottky diode, respectively. In Fig. 9 the capacitance C and the conductance G of the sample (normalized by the angular frequency ω) are plotted versus temperature for diode DOT25. At a reverse bias of $U_R = 4$ V, the capacitance decreases only slightly with decreasing temperature, corresponding to a location of the QW within the space-charge region. In this case, the QW is always depleted and no recharging occurs. However, if the $Si_{1-x}Ge_x$ layer is located in the neutral region, the diode capacitance $C_p(T)$ curve shows a characteristic decrease ΔC_p at lower temperatures. This situation is realized for reverse biases U_R smaller than 4 V in Fig. 9.

From the equivalent circuit for the space-charge region

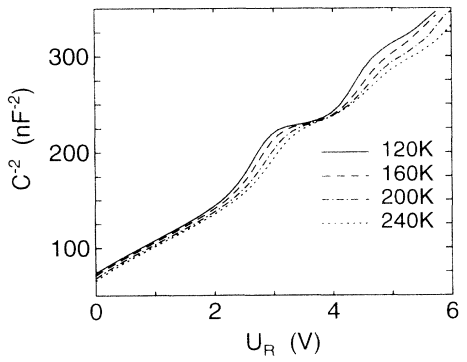

FIG. 8. Dependence of the capacitance C versus reverse bias U_R as plot $1/C^2$ versus U_R for 1-MHz measurements at different temperatures (QW with thickness $a = 3$ nm): $T = 120$ K (solid line), 160 K (dashed line), 200 K (dash-dot line), 240 K (dotted line).

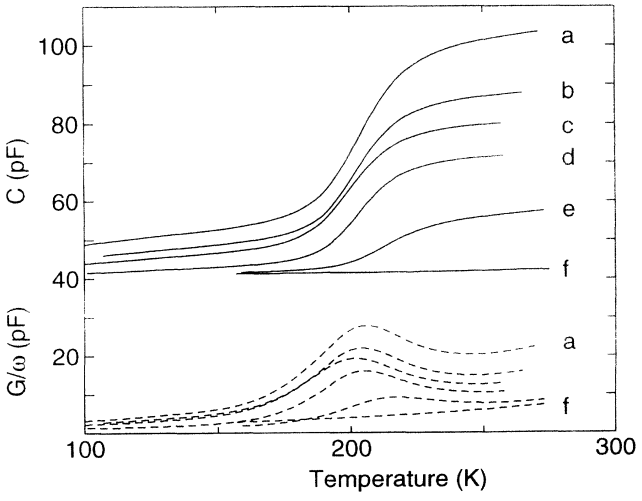

FIG. 9. Temperature dependence of the capacitance C (upper panel) and the normalized conductance G/ω (lower panel) for a measurement frequency $f = 1$ MHz at different reverse biases U_R: (a) $U_R = 0$ V, (b) 0.5 V, (c) 1.0 V, (d) 2.0 V, (e) 3.0 V, (f) 4.0 V. The area of the diode DOT25 was $A = 1.2\times10^{-3}$ cm^2.

of the n^+p diode or Schottky diode with the QW in the neutral region one obtains C_p and G_p (C and G measured in a parallel equivalent circuit) as a function of C_1, C_2, G, and $\omega=2\pi f$, where C_1 is the capacitance of the space-charge region, C_2 the capacitance of the QW and G the conductance across the QW.[8] The conductivity across the QW is high at high temperatures leading to $C_p^h=C_1$. In the opposite limit of low G the relation $C_p^l=C_1C_2/(C_1+C_2)$ applies. A maximum in $G_p(T)$ appears at $G^*=2\pi f(C_1+C_2)$.

The steplike change in C_p (Fig. 9) decreases for larger reverse bias and vanishes for $U_R > U_R^*$. For U_R^* the QW becomes depleted from confined carriers. $U_R^*=4$ V was obtained for the sample DOT25, and $U_R^*=2$ V for DOT26. The corresponding width $W(U_R^*)$ of the depletion region, obtained from CV measurements, lies between the positions of the QW and the interface between buffer and substrate, suggesting that the step in the $C_p(T)$ curves is indeed related to the $Si_{1-x}Ge_x$ layer. A second step in the 1 MHz $C_p(T)$ curve and a corresponding peak in $G_p(T)$ was observed at about 45 K independent of U_R. This signal is attributed to the freeze out of carriers in the substrate.

The temperature of the conductance peak for DOT25 does not change with increasing reverse bias up to 2 V (Fig. 9), suggesting that the QW is yet in the neutral region. From the temperature and frequency, dependence of the $G_p(T)$ peak information about the activation law of the conductance across the well is obtained. A shift to lower temperatures with decreasing frequency f was observed for the $G_p(T)$ peak and the corresponding step in $C_p(T)$. According to Eqs. (11) and (12) the temperature dependence of the conductance G of the QW is given by

$$G(T)\sim T^{1/2}v_c \exp[-(eU_0+E_{vb}-E_F)/k_BT] .$$

Hence, the resonance condition $G^*=2\pi f(C_1+C_2)$ determines the activation energy E_a. In Fig. 10 an Arrhenius plot of $f/T^{1/2}$ is shown for sample DOT25, leading to an activation energy of $E_a=(0.14\pm0.01)$ eV.

For the sample DOT26 with $x=0.25$, an activation energy $E_a=(0.15\pm0.01)$ eV was observed. Figure 11

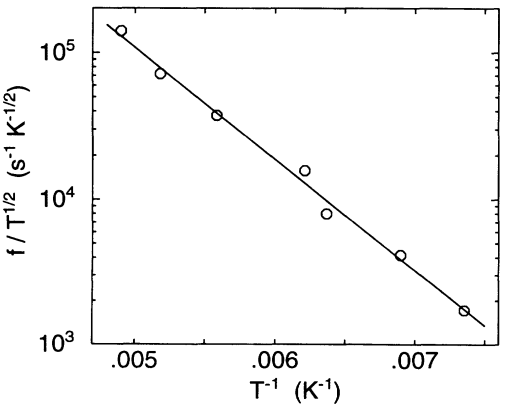

FIG. 10. Arrhenius plot of $f/T^{1/2}$ of the conductance peak obtained at $U_R=1$ V.

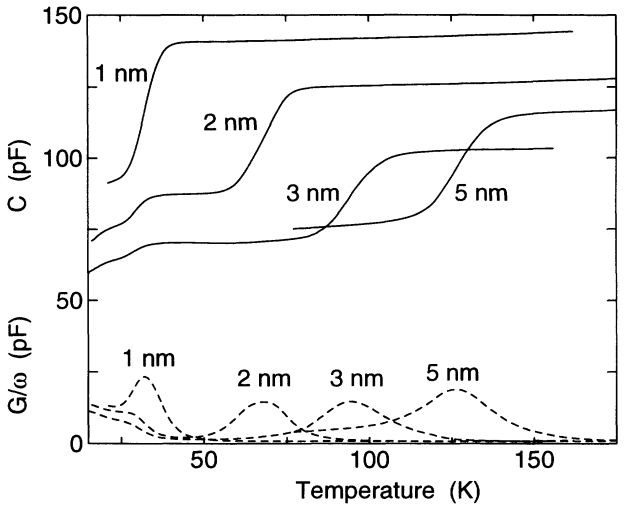

FIG. 11. Temperature dependence of the capacitance C (upper panel) and the normalized conductance G/ω (lower panel) for a measurement frequency $f=1$ MHz for QW's different thickness a 1, 2, 3, and 5 nm.

shows the $C_P(T)$ and $G_P(T)$ curves measured for the VG samples. The steplike change in $C_P(T)$ and the corresponding peak in $G_P(T)$ are shifted to lower temperatures for thinner wells. At temperatures below about 30 K a second step in the 1 MHz $C_P(T)$ curves was observed. Since no carrier freeze out occurs in the heavily doped p^+ substrate this step should be related to a freeze out of holes in the B-doped cap and buffer layers. From the temperature and frequency dependence of the $G_P(T)$ peak, the activation energy E_a of the conductance across the QW was measured. The values of the activation energy E_a obtained from the Arrhenius plot of $f/T^{1/2}$, are presented in Table I. Using the $C_P(T)$ dependence, the depletion width L_0 at the QW was estimated from the QW capacitance C_2, which is calculated from the capacitance values C_P^l and C_P^h direct below and above the $C_P(T)$ step, respectively, (Table I).

C. DLTS measurements

The reverse bias U_R^*, for which the QW becomes depleted, determines the voltage U_R which should be used for DLTS investigations of carrier emission from the QW, since in this case the influence of the electric field on carrier emission is minimal. The DLTS spectrum of the n^+p -mesadiode DOT25 taken at a measurement frequency of 1 MHz showed a strong peak with "negative" sign at $U_R < U_R^*$ ($U_R^*=4$ V) at about 200 K (Fig. 12). At this temperature, the sample capacitance $C_p(T)$ exhibited a steplike change during the DLTS measurement. The DLTS spectra of the WTi-Schottky diodes of the VG samples measured at $U_R < U_R^*$ also showed a DLTS peak at temperatures where the sample capacitance changes steplike. But in contrast to the n^+p-mesa diodes, the peaks have a "positive" sign. It is also noted that the

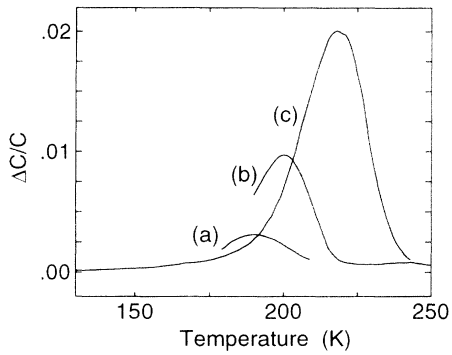

FIG. 12. Deep-level transient spectroscopy spectrum of DOT25 measured at the reverse bias $U_R = 3$ V and pulse bias $U_R = 0$ V obtained for different emission rate windows e_0: (a) 2.2, (b) 22, (c) 220 s^{-1}. The pulse width was $t_p = 50$ μs.

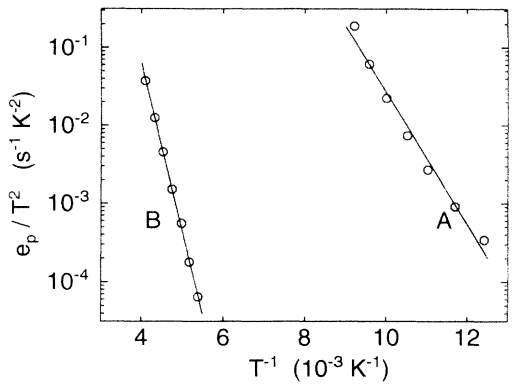

FIG. 14. Arrhenius plot of the normalized emission rate e_p/T^2 for the DLTS peaks A and B ($U_R = 4$ V, $U_1 = 0$ V, and $t_p = 50$ μs).

peak amplitude $\Delta C/C$ decreases considerably at lower emission rate windows.

For $U_R > U_R^*$, the region below the $Si_{1-x}Ge_x$ layer, i.e., the buffer contributes to the DLTS signal. Deep-level transient spectroscopy spectra of sample DOT25 obtained for $U_R = U_R^*$ showed two peaks (Fig. 13). Using DDLTS (double deep-level transient spectroscopy) depth profiling, the two peaks could be attributed to a region close to the $Si_{1-x}Ge_x$ layer. Arrhenius plots of the normalized hole emission rate e_p/T^2 revealed activation energies of $E_a = 0.17$ eV (A) and 0.42 eV (B) (Fig. 14) for the two levels in DOT25 (Fig. 13).

The concentration of level B varied quite considerably for different diodes of different Ge concentration. Relative concentrations $\Delta C/C$ of $(0.5...4)\times10^{-3}$ and $(0.5...3)\times10^{-2}$, respectively, were obtained for DOT25 and DOT26 implying that the concentration of level B was higher in samples with higher Ge concentration. For diodes with $\Delta C/C$ values of about 10^{-2}, a strong broadening of the peak shape was observed suggesting that the level B is due to process-induced structural defects. It should be mentioned that peak A with $\Delta C/C$ values of up to a few 10^{-3} has only been observed when the relative concentration $\Delta C/C$ of the deep level B was less than 10^{-3} Deep-level transient spectroscopy spectra of DOT25 measured down to 50 K did not show any other peaks than the peaks A and B. The DLTS peak A with an activation energy of $E_a = 0.17$ eV originates from the emission of holes from the QW region as proven by DDLTS depth profiling.

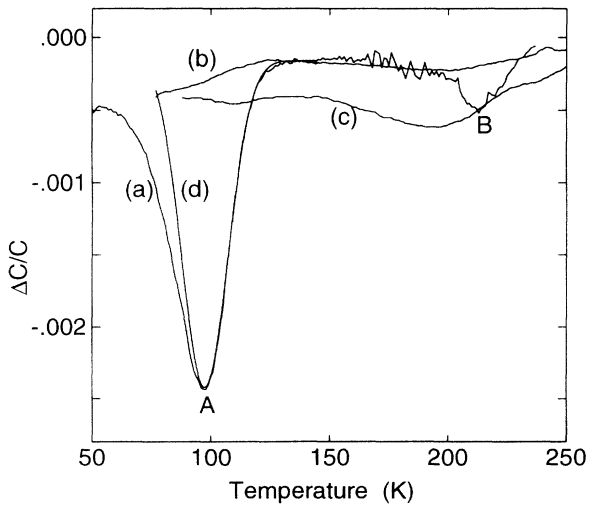

FIG. 13. Double deep-level transient spectroscopy spectra of DOT25 obtained with at rate window $e_0 = 220$ s^{-1}, pulse width $t_p = 50$ μs, reverse bias $U_R = 4$ V, and different pulses biases U_1 and U_2: (a) $U_1 = 1.5$ V, $U_2 = 2$ V, (b) $U_1 = 0$ V, $U_2 = 0.5$ V, and (c) $U_1 = 3.0$ V, $U_2 = 3.5$ V. The peak (d) was simulated assuming an activation energy $E_a = 0.17$ eV and a Gaussian distribution of E_a with $\Delta E_a = 15$ meV.

The emission rate e_T of the hole emission from QW's is given by Eq. (5) implying that the temperature dependence of the preexponential factor differs from the T^2 dependence usually assumed for deep centers in bulk semiconductors. For large wells the preexponential factor is nearly temperature independent. The activation energy has therefore been recalculated from the Arrhenius plot of e_p versus $1/T$ giving an activation energy of $E_a = (0.18 \pm 0.02)$ eV and a preexponential factor $(2v_c/\lambda_T f) = 5\times10^{11}$ s^{-1}. The parameters obtained for the QW suggest an occupation factor f of about 3 leading to a capture velocity v_c of about 6×10^5 cm/s in agreement with our calculation.[11,12] This supports the assumption that hole emission from the QW has been observed. The shape of the DLTS peak simulated with the parameters taken from the Arrhenius plot was narrower than the measured peak shape. However, assuming a Gauss distribution of the activation energy E_a with $\Delta E_a = 15$ meV, good agreement with the measured peak shape was obtained (Fig. 13).

At high electric fields the effective barrier is lowered due to tunneling effects. For the effective lowering one obtains from Eq. (17) $\Delta E_{tu} = \hbar^2 e^2 F^2/24$ m $(k_B T)^2$, leading to a value of about 4 meV for p-Si at $T = 100$ K and

TABLE II. Dependence of the peak temperature T_p on the reverse bias U_R. Parameter of the DLTS measurement: rate window $e_0=22\ s^{-1}$, pulse biases $U_1=2$ V and $U_2=3$ V; pulse duration $t_{p1}=t_{p2}=500\ \mu s$.

U_R/V	4	5	6
T_p/K	94	92	87

an electric field of $F=5\times10^4$ V/cm, which shows that the potential barrier lowering is not large for such fields.

For higher electric fields, the activation energy E_a is expected to decrease. In the case of DLTS measurements with given rate window e_0 for the emission rate e_T, the peak temperature T_p of the DLTS peak indeed decreased with increasing reverse bias U_R, as shown in Table II. Increasing U_R from 4 to 6 V, corresponding to an electric field F of about 10^5 V/cm at the $Si_{1-x}Ge_x/Si$ interface of the QW, the activation energy decreased by $\Delta E_a=20$ meV. This value is somewhat smaller than the theoretically estimated shift of 40 meV which included the effect of carrier tunneling. The surface concentration n_w of captured holes is obtained from the relation $\Delta C/C=n_wL/(2N_AW^2)$,[4] where L is the depth of the QW layer, W is the width of space-charge region, and N_A is the acceptor concentration in the buffer layer. Using $N_A=1\times10^{17}\ cm^{-3}$ and a pulse duration $t_p=50\ \mu s$ one obtains $n_w=2\times10^{10}\ cm^{-2}$.

The capture of holes into the QW was investigated by studying the dependence of the DLTS peak $\Delta C/C$ on the filling pulse t_p. It turned out that the relative signal $\Delta C/C$ of the DLTS peak depended approximately logarithmically on t_p (Fig. 15). Plotting $\Delta C/C$ versus $\ln(t_p/t_{0)}$ and extrapolating ΔC to 0, a characteristic time

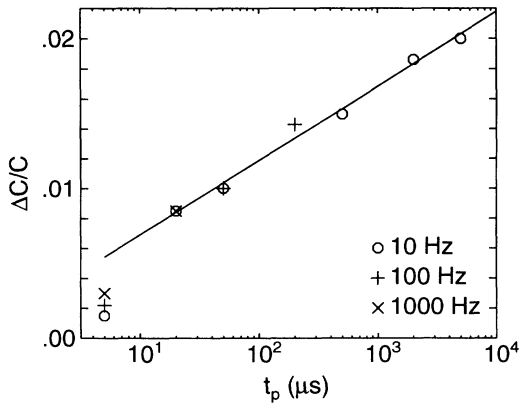

FIG. 15. Dependence of the relative DLTS signal $\Delta C/C$ on the pulse width t_p. Double deep-level transient spectroscopy measurements were performed with a reverse bias $U_R=4$ V and pulse biases $U_1=2$ V and $U_2=3$ V (rate window e_0: o, $22\ s^{-1}$; +, $220\ s^{-1}$; ×, $2200\ s^{-1}$).

$t_0=10^{-6}$ s was obtained. Theoretical considerations of the capture process (Sec. II D) suggest a much shorter time constant for capture processes of confined two-dimensional holes in the QW. Furthermore, the calculated concentration $n_w=10^{11}\ cm^{-2}$ of holes in the QW (Table III) is considerably higher than the estimated two-dimensional carrier concentration related to the DLTS peak A. Assuming a valence-band offset $\Delta E_v=0.14$ eV for sample DOT25, which corresponds to the theoretical value for the band offset, one can relate the measured activation energy $E_a=0.18$ eV to states in the QW region about 40 meV below the bottom of the well. That is why the DLTS peak A is more likely to be due to defect states in the QW region than due to direct

TABLE III. Results of self-consistent calculations for the confinement energy E_1, the Fermi energy E_F, the effective barrier $eU_0+E_{vb}-E_F$, the depletion width L_0, and the two-dimensional hole concentration.

a (nm)	d_{sp} (nm)	x	N_A ($10^{17}\ cm^{-3}$)	T (K)	ΔE_v (meV)	E_1 (meV)	$-E_F$ (meV)	$eU_0+E_{vb}-E_F$ (meV)	L_0 (nm)	n_w ($10^{11}\ cm^2$)
30	50	0.17	2.5	160	136	11	46	155	40	1.2
				160	122	10	46	144	39	0.9
30	50	0.25	1.8	150	200	15	46	204	44	2.7
				150	180	14	46	187	43	2.4
1	30	0.25	2.8	30	200	149	23	52	39	0.6
				30	160	125	23	39	37	0.2
2	30	0.25	2.0	60	200	74	26	121	43	3.2
				60	160	66	26	92	41	2.1
				110	200	75	35	125	42	3.1
3	30	0.25	2.0	90	200	50	31	144	44	3.9
				90	160	46	31	112	42	2.8
				120	200	50	37	147	43	3.8
5	30	0.25	2.0	120	200	26	37	168	45	4.5
				120	160	23	37	135	42	3.4
				160	200	26	48	173	44	4.2
20	30	0.25	3.0	130	200	19	37	186	42	4.8
				130	160	15	37	153	40	3.6
				190	200	18	53	200	42	4.1

emission from the two-dimensional hole gas in the QW. Further investigations are needed to clarify this point.

Deep-level transient spectroscopy measurements were also performed on VG samples with a thinner cap layer (removed by etching) to obtain optimal conditions for the DLTS investigations of the QW. The relative concentration $\Delta C/C$ of deep levels with up to about few 10^{-3} was somewhat higher that the one observed for the n^+p-mesa diode DOT25. Despite low leakage current of the investigated Schottky diodes, the DLTS spectra have not shown any peak which could be related to hole emission from the QW.

IV. RESULTS AND DISCUSSION

The parameters of the $Si/Si_{1-x}Ge_xSi$ layers, e.g., the thickness a of the undoped $Si_{1-x}Ge_x$ layer, the Ge concentration x, the thickness d_{sp} of the undoped spacers, as well as the acceptor concentrations N_{A1} and N_{A2} in the boron-doped cap layer and the buffer layer, respectively, are given in Table I together with a summary of the experimental results. The QW structures were prepared with undoped spacers adjacent to the $Si_{1-x}Ge_x$ layer in order to suppress a possible tunneling of holes through the barriers via shallow acceptor states.

The concentration of holes n_w and the depletion width L_0 obtained from $C(U_R)$ and $C(T)$ measurements are given together with the activation energy E_a of the conductance across the QW determined by admittance spectroscopy. The temperatures, for which the experimental results were obtained, are also given. In those cases where a carrier emission from the QW region has been observed by DLTS, the activation energy is listed.

The activation energy E_a of the conductance across the QW should be compared with the calculated barrier $(eU_0+E_{vb}-E_F)$. The theoretical values of $(eU_0+E_{vb}-E_F)$ as well as of n_w and L_0 are presented in Table III for temperatures corresponding to the experimental conditions. Table III gives also the Fermi energy E_F and the confinement energy E_1 of the first level of the heavy holes in the QW. An averaged concentration $N_A=(N_{A1}+N_{A2})/2$ was assumed, because the results do not depend very sensitively on the acceptor concentration. Calculations were carried out for two different values of the valence-band offset. The value of $\Delta E_v=136$ meV and $\Delta E_v=200$ meV for $x=0.17$ and 0.25, respectively, correspond to the theoretical values of the band offset as discussed in Sec. II. As a test for the sensitivity of the determined QW characteristics on the material parameter ΔE_v the calculations were repeated for reduced values $\Delta E_v=122$ and 160 meV, respectively. Samples for which the two-dimensional carrier concentration in the well was determined from CV measurements are also included in Table III together with calculated data close to the temperature of the CV measurements.

The experimental values of the activation energy E_a obtained from admittance spectroscopy for the VG samples with $x=0.25$ and $a=1,\ldots,5$ nm seem to be in very good agreement with theoretical values of $(eU_0+E_{vb}-E_F)$ assuming a lower band offset of $\Delta E_v=0.16$ eV. It should be mentioned, however, that the actual barrier height is strongly dependent on the abruptness of the $Si/Si_{1-x}Ge_x$ interfaces. To check the effect of atomic intermixing at the interfaces, the activation energies were recalculated assuming a smeared out valence-band discontinuity. The valence-band edge near an interface at $x=x_0$ was modeled by

$$E_v(x)=E_{vb}+\Delta E_v\left[1+\exp\left|\frac{x-x_0}{b}\right|\right]^{-1}.$$

The calculated values for a characteristic length $b=0.5$ nm, a measure of the smearing out effect, are given in Table IV. The barriers $eU_0+E_{vb}-E_F$ calculated for $b=0.5$ nm and $\Delta E_v=0.20$ eV are again in good agreement with the results obtained from the admittance spectroscopy measurements for the VG samples with $x=0.25$ and $a=1\ldots5$ nm. Since the microscopic composition near the interfaces is unknown, we are left with an uncertainty about the abruptness of the band discontinuity at the interfaces. Assuming $b=0,\ldots,0.5$ nm, one obtains from the comparison of the measured activation energies E_a with the calculated barrier heights $eU_0+E_{vb}-E_F$ a valence-band discontinuity $\Delta E_v=0.18\pm0.02$ eV for the $Si/Si_{0.75}Ge_{0.25}/Si$ system.

It is worth mentioning that the calculated barriers $eU_0+E_{vb}-E_F$ for the discussed thin wells at low temperatures are well approximated by the value ΔE_v-E_1. This is because the Fermi level is closely pinned to the bottom of the first heavy-hole subband E_1 in thin QW's at low temperatures. The relation $eU_0+E_{vb}-E_F\approx\Delta E_v-E_1$ allows a simple interpretation of the activation energies measured by admittance spectroscopy in terms of band discontinuities ΔE_v.

For thicker QW's (≥ 20 nm), in the case of VG samples, and for higher Ge concentrations ($x=0.25$), in the case of DOT samples, the activation energy E_a could be influenced by the considerably higher defect concentration observed by DLTS. For the n^+p-mesa diode

TABLE IV. Calculated QW characteristics assuming an intermixing at the interfaces ($b=0.5$ nm).

a (nm)	d_{sp} (nm)	x	N_A (10^{17} cm^{-3})	T (K)	ΔE_v (meV)	E_1 (meV)	$-E_F$ (meV)	$eV_0+E_{vb}E_F$ (meV)	L_0 (nm)	n_w (10^{11} cm^{-2})
1	30	0.25	2.8	30	200	163	23	41	38	0.3
2	30	0.25	2.0	60	200	109	26	90	41	2.0
3	30	0.25	1.8	90	200	79	31	119	42	3.0
5	30	0.25	2.0	120	200	39	37	157	44	4.2

DOT25 ($x=0.17$) with low defect concentration, a band offset $\Delta E_v=0.12$ eV was estimated from E_a assuming 50-nm undoped spacers. However, due to a relatively high boron background contamination in the MBE equipment used for the layer deposition of DOT samples, the assumption of undoped spacers is questionable. According to the CV measurements, an acceptor concentration as high as 10^{17} cm^{-3} in the nominally undoped regions cannot be excluded for these samples. Assuming a constant acceptor concentration $N_A=10^{17}$ cm^{-3} the measured activation energy $E_a=0.14$ eV is consistent with the assumption of a valence-band offset $\Delta E_b=0.16$ eV. Regarding the uncertainty of the acceptor concentration in sample DOT25, a valence-band offset $\Delta E_v=0.14\pm0.02$ eV is estimated for $x=0.17$.

A DLTS peak related to hole emission from the QW region was obtained only for the best n^+p-mesa diodes with $x=0.17$. The corresponding activation energy $E_a=0.18\pm0.02$ eV obtained from the temperature dependence of the emission rate is considerably higher than the expected band offset $\Delta E_v=0.14$ eV for $x=0.17$. The peak should therefore be related to states about 40 meV below the bottom of the well. These states could arise from a background boron contamination in the QW. The emission process related to the DLTS signal from the QW is assumed to be a two-step process consisting of the ionization of the shallow acceptors and the emission of holes from the QW.

The question arises why no evidence was found for hole emission from the QW in case of Schottky diodes. It is argued that for the n^+p-mesa diodes the lateral distribution of the surface potential may keep the holes in the QW region beneath the n^+ contact when switching the bias to the depletion mode. On the other hand, it is assumed that for the Schottky diodes the holes could be swept from the QW region beneath the Schottky contact laterally before hole emission across the barrier can occur.

V. SUMMARY

Capture and emission processes of holes in p-type $Si/Si_{1-x}Ge_x/Si$ QW's were studied by admittance spectroscopy and DLTS. It is shown that a detailed understanding of the basic processes of carrier capture and emission is essential for a reliable interpretation of the experimental data. The theory of carrier capture and emission presented in this paper allows the study of equilibrium and nonequilibrium conditions taking into account external electric fields as well as the local electric field induced by confined holes. The potential barriers at the QW formed by confined holes were calculated solving self-consistently Schrödinger's and Poisson's equations. The temperature dependence of these potential barriers and of the Fermi level determines the activation energy E_a of the conductance across the QW.

In order to minimize leakage currents across the QW layer, n^+p-mesa diodes and WTi-Schottky diodes with a buried $Si_{1-x}Ge_x$ layer were used for the study of capture and emission processes of holes. The dependence of the activation energy E_a of conductance across the QW on the thickness of the QW, which was observed for perfect $Si/Si_{1-x}Ge_x/Si$ QW with $x=0.25$, is in correspondence with the theoretical calculations. The valence-band offset of $\Delta E_v=0.18\pm0.02$ eV obtained from admittance spectroscopy is in agreement with the calculated values[20] and those obtained from photoemission measurements[21] which gave $\Delta E_v=0.20$ eV $x=0.25$.

Hole emission from the QW region was observed for n^+p-mesa structures with $x=0.17$ in DLTS, but not for the investigated Schottky diodes. The observed DLTS peak for n^+p-mesa diodes was attributed to carrier emission from states about 40 meV below the bottom of the QW.

ACKNOWLEDGMENTS

We would like to express our gratitude to B. Dietrich for the Raman measurements. The help of K. Tittelbach-Helmrich in the automation of the capacitance measurements is acknowledged. We are indebted to H. Schneider for the preparation of the WTi-Schottky diodes and to R. Winkler for help in sample preparation.

APPENDIX A

The highest valence bands of silicon and germanium can be described by a Luttinger Hamiltonian using the three independent parameters γ_1, γ_2, γ_3,

$$H_L=-\frac{\hbar^2k^2}{2m_0}(\gamma_1+2\gamma_2)+\frac{3\gamma_2\hbar^2}{2m_0}\sum_i\hat{L}_i^2k_i^2 + \frac{\gamma_3\hbar^2}{2m_0}\sum_{i\neq j}\{\hat{L}_i\hat{L}_j\}k_ik_j+H_{so}\ , \tag{A1}$$

where m_0 is the mass of a free electron, k_i are the wave-number components, and $\{\hat{L}_i\hat{L}_j\}=\hat{L}_i\hat{L}_j+\hat{L}_j\hat{L}_i$, and $\hat{L}_j$ are the angular-momentum $\frac{3}{2}$ matrices. The Hamiltonian H_{so} accounts for the spin-orbit interaction.

The general effect of strain on the valence-band complex is to provoke a shift of the $J=\frac{3}{2}$ and $J=\frac{1}{2}$ states as well as a splitting of the doubly degenerate $J=\frac{3}{2}$ manifold described by the three deformation potentials a, b, and d,

$$H_{st}=\sum_i(a+2b)\epsilon_{ii}\hat{1}-3b\sum_i\hat{L}_i^2\epsilon_{ii}-\sqrt{3}d\sum_{i\neq j}\{\hat{L}_1\hat{L}_j\}\epsilon_{ij}\ , \tag{A2}$$

where ϵ_{ij} are the components of the strain tensor. For strained layers pseudomorphically grown on (001) substrates the strain tensor is diagonal and has the form

$$\epsilon_{xx}=\epsilon_{yy}=\epsilon,\quad \epsilon_{zz}=-K\epsilon\ , \tag{A3}$$

where the factor K is given by the elastic constants

$$K=\frac{2c_{12}}{c_{11}}\ . \tag{A4}$$

The highest valence band in strained $Si_{1-x}Ge_x$ matched on Si(001) is the $|J=\frac{3}{2},J_z=\frac{3}{2}\rangle$ state where the z axis was

chosen as the axis of quantization of the angular momentum. Starting from a spherical Luttinger Hamiltonian [$\gamma_2=\gamma_3=\gamma$ in Eq. (A1)] one obtains the effective masses

$$m_z=\frac{1}{\gamma_1-2\gamma_2},\quad m_x=m_y=\frac{1}{\gamma_1+\gamma_2} \tag{A5}$$

for the topmost valence band. Since $m_z=m_{\mathrm{HH}}$ is equal to the mass of the heavy hole we call this band the heavy-hole band in the strained layer. However, the mass m_x controlling the motion within the quantum well layer is close to the light-hole mass $m_{\mathrm{LH}}=1/(\gamma_1+2\gamma_2)$ in the unstrained layer. This has important consequences on the in-plane transport properties of the quantum well. Similarly, the light-hole band in the strained layer has a small mass in z direction and a bigger in plane mass.

In addition to the effect of strain on the band structure, we have to consider the confinement of holes in the $Si_{1-x}Ge_x$ layer representing a quantum well. Usually the quantization of holes described by a Luttinger-type Hamiltonian requires the solution of a coupled system of differential Schrödinger equations for the $J=\frac{3}{2}$ manifold. However, in the case of strained $Si_{1-x}Ge_x$ wells with $x\simeq 0.20$ and well widths $a\simeq 30$ nm, which are considered here the splitting of the light- and heavy-hole bands due to strain is much bigger than the confinement energy. Therefore, the system of differential equations decouples and the individual hole bands are described by Schrödinger-type equations with anisotropic effective masses. For the calculation of confined hole levels in the quantum well we subsequently solve the one band Schrödinger equations and the Poisson equation for the resulting charge density until self-consistency is achieved. Changes in the exchange-correlation potential due to carrier confinement have not been considered here.

As verified by Van de Walle and Martin[20] the strain-dependent band alignment of the valence bands at a Si/Ge interface can be described as the sum of a strain independent part ΔE_v^0 and the strain dependent shift $\delta_{\mathrm{st}}E_v$ of the individual bands $v=$HH, LH, SO

$$\Delta E_v=\Delta E_v^0+\delta_{\mathrm{st}}E_v\ . \tag{A6}$$

For the dependence of the band discontinuities at $Si/Si_{1-x}Ge_x$ interfaces on the alloy composition x a linear dependence of ΔE_v^0 on x is assumed.

APPENDIX B

The thermally activated tunneling is considered for carriers (e.g., holes) confined in a QW with parabolic barriers

$$V(z)=eU_0\left[\frac{z-L_0}{L_0}\right]^2 \tag{B1}$$

(see Fig. 2). Within the quasiclassical approximation the tunneling probability of a carrier in the quasistationary state E_m is given by

$$W(E_n)=\frac{2D(E_m)}{T(E_m)}\ , \tag{B2}$$

where

$$D(E_m)=\exp\left[-2\frac{\sqrt{2m}}{\hbar}\int_0^{z_2}\sqrt{\Delta E_v-E_m+V(z)-eU_0}\,dz\right] \tag{B3}$$

is the transmission coefficient of the barrier for a particle in the state E_m and $T(E_m)$ is the classical oscillation period in the state E_m [Eq. (14)]. The limit of integration z_2 is determined by the condition $\Delta E_v-E_m+V(z_2)-eU_0=0$. Since the probability $P(E_m)$ of the occupation of the state E_m decreases with the energy E_m as $\exp(-E_m/k_BT)$, there is an optimal tunneling energy for which the exponent index of the product $P(E_m)D(E_m)$ is minimal. It is this energy

$$E_{\mathrm{opt}}=\Delta E_v-eU_0\tanh^2\left[\frac{E_t}{k_BT}\right]\ , \tag{B4}$$

where

$$E_t=\left[\frac{eU_0\hbar^2}{2mL_0^2}\right]^{1/2} \tag{B5}$$

that determines the thermal emission rate. Using the relation

$$L_0=\left[\frac{2U_0\epsilon\epsilon_0}{eN_A}\right]^{1/2} \tag{B6}$$

for the depletion region the characteristic energy E_t can be written as in Eq. (13). For the thermal emission flux density we get

$$j_{em}=\sum_m\frac{2D(E_m)P(E_m)}{T(E_m)}\simeq\frac{2mk_BT\tilde{\nu}}{T(E_{\mathrm{opt}})\pi\hbar^2}\exp\left[\frac{E_F}{k_BT}-\frac{eU_0}{E_t}\tanh^2\left[\frac{E_t}{k_BT}\right]\right]\ . \tag{B7}$$

The factor $\tilde{\nu}$ is the number of quasistationary levels situated in the "saddle" width

$$\Delta E=eU_0\frac{\sinh^{1/2}(E_t/k_BT)}{\cosh^{3/2}(E_t/k_BT)} \tag{B8}$$

near the optimal tunneling energy. If we introduce the thermal emission rate e_{tu} as the emission probability of carriers in the first subband E_1, we obtain Eq. (13) of the main text.

[1] *Heterojunction Band Discontinuities: Physics and Device Applications,* edited by F. Capasso and G. Margaritondo (Elsevier, Amsterdam, 1987).

[2] D. V. Lang, in *Heterojunction Band Discontinuites: Physics and Device Applications* (Ref. 1), p. 377.

[3] S. M. Sze, *Physics of Semiconductor Devices* (Wiley, New York, 1981), p. 255.

[4] N. Debbar, Dipankar Biswas, and Pallab Bhattachrya, Phys.

Rev. B **10**, 1058 (1989).
[5]X. Letarte, D. Stievenard, and E. Barbier, Appl. Phys. Lett. **58**, 1047 (1991).
[6]L. Vescan, R. Apetz, and H. Lüth, J. Appl. Phys. **73**, 7427 (1993).
[7]K. L. Jiao and W. Anderson, J. Appl. Phys. **73**, 271 (1993).
[8]K. Nauka, T. I. Kamins, J. E. Turner, C. A. King, J. L. Hoyt, and J. F. Gibbons, Appl. Phys. Lett. **60**, 195 (1992).
[9]G. Grumt and R. Pickenhain, Solid State Commun. **73**, 257 (1990).
[10]C. Jain and W. Hayes, Semicond. Sci. Technol. **6**, 547 (1991).
[11]I. N. Yassievich, K. Schmalz, and M. Beer, Semicond. Sci. Technol. (to be published).
[12]M. Beer, K. Schmalz, and I. N. Yassievich (unpublished).
[13]K. Schmalz, H. Rücker, I. N. Yassievich, H. G. Grimmeiss, B. Dietrich, H. Frankenfeld, W. Mehr, H. J. Osten, and P. Schley, Solid-State Electron. **37**, 945 (1994).
[14]C. Weisbuch and B. Vinter, *Quantum Semiconductors Structures* (Academic, New York, 1991), p. 20.
[15]V. N. Abakumov, V. I. Perel, and I. N. Yassievich, *Nonradiative Recombination in Semiconductors* (North-Holland, Amsterdam, 1991).
[16]H. J. Osten, G. Lippert, and J. Klatt, J. Vac. Sci. Technol. B **10**, 1151 (1992).
[17]B. Dietrich, E. Bugiel, J. Klatt, G. Lippert, T. Morgenstern, H. J. Osten, and P. Zaumseil, J. Appl. Phys. **74**, 3177 (1993).
[18]X. Letartre, D. Stievenard, and E. Barbier, J. Appl. Phys. **69**, 7912 (1991).
[19]K. Kreher, Phys. Status Solidi A **135**, 597 (1993).
[20]C. G. Van de Walle and R. M. Martin, Phys. Rev. B **34**, 5621 (1986).
[21]W. X. Ni and G. V. Hansson, Phys. Rev. B **42**, 3030 (1990).

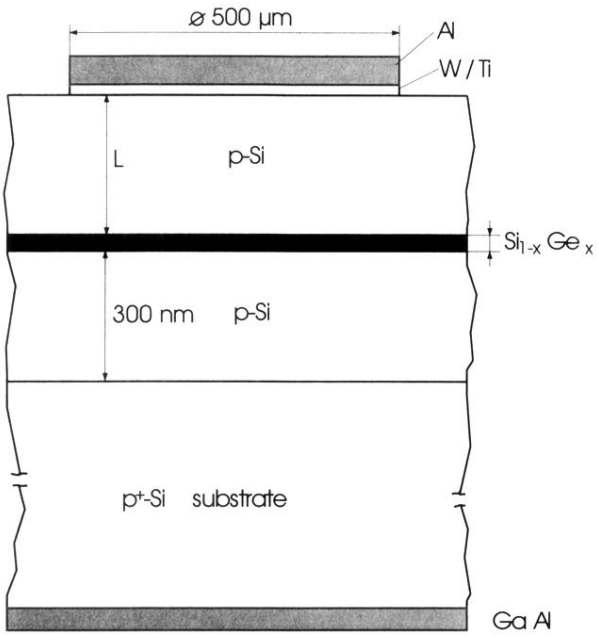

FIG. 6. Schematic picture of the WTi-Schottky diode used (VG samples).